NOVEL GOLD DEPORTMENT TECHNIQUE - APPLICATIONS FOR COMPLEX COPPER-GOLD AND REFRACTORY GOLD ORES

Aparup Chattopadhyay[1], Stamen Dimov[2], Brian Hart[2], and Barun K. Gorain[3]

[1]*Integrated Process Mineralogy Solutions Inc.*
5646 Patron Cove
Mississauga, Ontario, Canada L5M 7G4
*(*Corresponding author: achattopadhyay@ipmins.com)*

[2]*Surface Science Western, Western University,*
999 Collip Circle, London, Ontario, N6G 0J3
(sdimov@uwo.ca, bhart@uwo.ca)

[3]Barrick Gold Corporation
Suite 3700, 161 Bay St, Canada Trust Tower
Toronto, Ontario, Canada M5J 2S1
(bgorain@barrick.com)

ABSTRACT

A novel gold deportment technique has been developed for complex copper-gold and double refractory gold ores using state-of-the-art technology. Characterization of these ores is a challenging task due to low copper and gold grades in ores, presence of both primary and secondary copper sulfide phases and variable proportion of visible and invisible gold in different sulfides and iron oxide phases.

Double refractory ores are mainly composed of silicates and carbonates with moderate clay and mica, and minor amounts of sulfides and organic carbonaceous matter. Gold mostly occurs as "invisible gold" (sub-microscopic gold) as solid solution or as colloidal-sized particles in different sulfides and other phases. The dominance of invisible gold and presence of highly preg-robbing and finely disseminated carbonaceous matter adversely affects gold recovery in flotation and leach circuits. Characterization of this carbonaceous matter, commonly known as TCM and quantification of gold associated within TCM, along with different sulfide and oxide phases is highly complex and challenging.

Studies were initiated on various complex ore deposits and also on samples representing various process streams. This paper presents the development of a systematic approach to diagnostic metallurgy using state-of-the-art optical and automated mineralogy techniques, namely, micro-probe, dynamic SIMS and TOF-SIMS analysis for quantification of invisible and visible precious metal content in various species. The relevance of the mineralogy characterization to metallurgy will also be discussed in this paper.

KEYWORDS

Gold deportment, complex copper-gold ore, double refractory ores, carbonaceous matter, preg-robbed surface gold, gold mineralogy, gold processing, ore characterization, diagnostic metallurgy

INTRODUCTION

A novel characterization methodology has been developed for complex copper-gold and double refractory gold ores using state-of-the-art technology for quantitative gold and copper deportment study. The characterization of these ores is a challenging task due to low copper and gold grades in ores, presence of both primary and secondary copper sulfide phases, presence of variable proportion of preg-robbing carbonaceous matter (TCM) with sulfide inclusions, visible and invisible gold in different sulfides phases (pyrite, chalcopyrite, chalcocite and bornite) and iron oxide phases (magnetite, hematite and goethite). A study was initiated on various ore deposits and also on samples representing various processing streams of pilot plant batches such as flotation circuits (concentrate and tailings) and leaching circuits (POX/CIL residue and CIL residue).

This paper discusses the deportment characterization methodology by presenting results from investigations on samples from flotation (feed, concentrate, scavenger/rougher tail samples) and leach circuits (feed, POX/CIL residue and CIL residue). These samples represent the key streams for a typical copper-gold flotation and gold leaching flow sheet. Key objectives of this investigation were: to identify and quantify visible and invisible gold along with understanding the morphology and liberation of gold associated with various sulfides, Fe-oxides and non-sulfide gangue species. In addition, the aim of this study was also to relate the mineralogical and gold deportment information to metallurgical performance.

A variety of gold deposit types related to porphyry copper mineralization, including skarns, polymetallic veins and replacements, and epithermal veins. Sillitoe and Perelló (2005) described iron-oxide-copper-gold, copper-bearing volcanogenic massive sulfide deposits, and copper skarns (copper-zinc-molybdenum-silver) spatially associated with porphyry copper belts in the Andes. Jensen and Barton (2000) described alkalic porphyry systems with intermediate-sulfidation epithermal base-metal-gold-telluride deposits. Gold deportment studies for these ores are different and easier than complex copper-gold and double refractory gold ores.

The gold ore body in this investigation is in north-eastern Nevada, United States and is commonly known as a Carlin type deposit, after the Carlin ore body. Mineralization covers an extensive area and numerous orebodies have been localized by complex structural and lithological controls. Most of the economic gold mineralization is hosted in limy to dolomitic mudstones. The characteristics of the host rocks that are believed to enhance their favourability to gold deposition include the presence of reactive carbonate, porosity, permeability and the presence of iron, which can be sulfidized to form auriferous pyrite (Bettles, 2002). Most of gold at Goldstrike is located in arsenian pyrite overgrowths or pre-ore pyrite (Arehart et al., 2003).

Naturally occurring organic carbon or TCM is found in many of the ores within the Carlin trend and has the ability to adsorb gold cyanide from the leach solution, a process commonly known as preg-robbing (Hausen & Bucknam, 1984; Stenebraten, Johnson, & McMullen, 2000; Helm, Vaughan, Staunton, & Avraamides, 2009). The proportion of TCM in these ores ranges from absent to 8.5% with varying preg-robbing activities which result in gold recoveries ranging from approximately 20–90% (Stenebraten et al., 2000).

The gold deportment study aimed to: i) gain a clear understanding of the gold distribution in sulfides, iron oxides and carbonaceous matter, ii) to understand the morphology of the carbonaceous matter and distribution of gold in the carbonaceous matter, and iii) evaluate the gold loss during removal of carbonaceous matter.

METHODOLOGY

Barrick Gold Corporation provided representative samples of the key flotation and leach circuits as discussed in the previous section. These samples were split from as-received samples for polished section preparation for bulk mineralogy by optical and quantitative evaluation of mineralogy by scanning

electron microscopy (QEMSCAN) modal and liberation analysis, and also for carrying out chemical assays as shown in flow chart diagram (Figure 1). This type of representative mineralogy sampling of gold, TCM and sulfide phases reveal more precise gold distribution data.

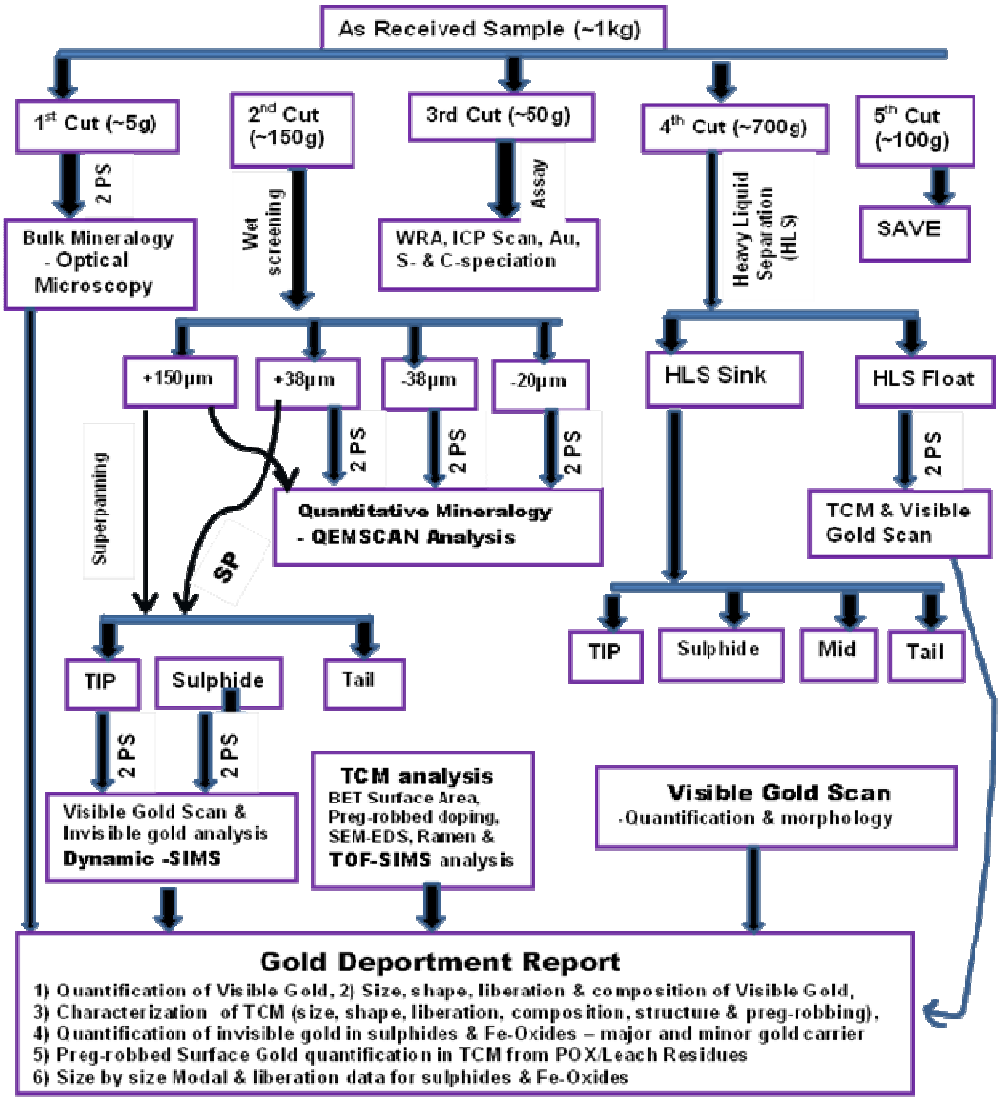

Figure 1 – Flow-chart diagram of novel gold deportment technique (Chattopadhyay & Gorain, 2014)

MINERALOGY

Bulk Mineralogy

The mineralogical findings presented in this paper are based on two feed composite samples and five processed products from flotation/CIL leach circuits. The bulk mineralogy and quantitative mineral analysis were carried out by optical microscopy, X-ray powder diffraction (XRD) and QEMSCAN analysis. The bulk mineralogy of the rougher feed and tailings samples was similar, mainly composed of quartz, plagioclase and mica with minor amount of Fe-oxides and a minor to traces of Cu-sulfide phases. cleaner tails were mainly composed of pyrite, mica and quartz while the final concentrate was dominantly composed of chalcopyrite with minor amounts of other Cu-sulfides and pyrite (Plate 1). The bulk mineralogy of three CIL leach stream samples was similar, mainly composed of quartz with moderate

amounts of dolomite, mica and clay (kaolinite). Minor to trace amounts of pyrite/arsenian pyrite, sulfate, carbonaceous matter (TCM and graphitic carbonaceous matter), calcite, Fe-oxides, sphalerite, chalcopyrite and galena were noted. The quantitative mineral analysis data are presented in Tables 1A–1B.

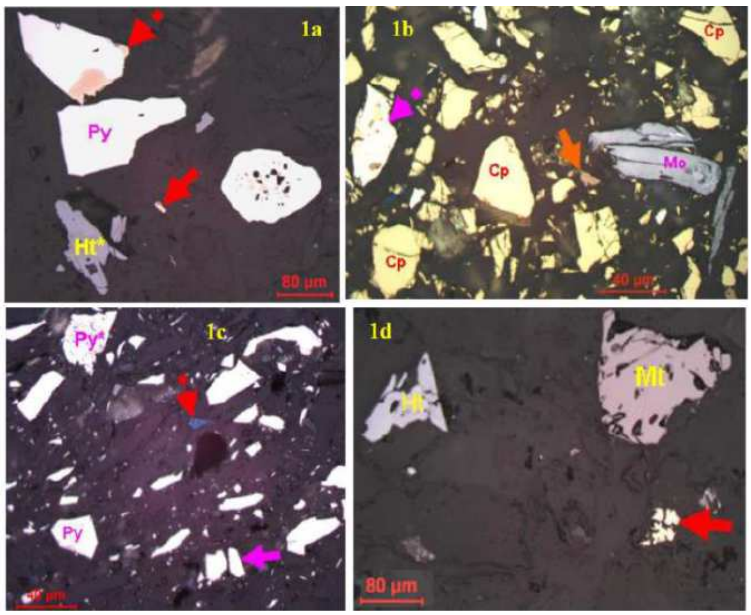

Plate 1 – Photomicrographs of polished sections from flotation stream samples showing association of chalcopyrite/covellite (Cp/red arrow), bornite (orange arrow), pyrite (py/pink arrow), molybdenite (Mo), hematite (Ht) and magnetite (Mt) in: a) feed sample, b) concentrate, c) cleaner tails, and d) rougher tails

Table 1A – Mineral distribution data used for gold deportment study from flotation stream

Mineral Mass	Sample ID			
(in wt%)	Rougher Feed	Rougher Tails	Cleaner Tails	Final Conc.
Chalcopyrite	1.8	0.1	0.1	85.4
Bornite	0.1	0.0	0.0	4.0
Covellite	0.1	0.0	0.0	3.1
Pyrite	4.3	0.6	22.6	6.3
Other Sulfides	0.2	0.0	2.5	0.2
Quartz	38.9	41.8	20.8	0.1
Plagioclase	14.5	16.6	8.8	0.0
K-Feldspars	3.4	3.8	0.9	0.0
Amphibole	0.6	0.4	2.0	0.2
Micas	23.7	25.0	25.6	0.3
Chlorite	5.0	5.1	4.6	0.1
Clays	3.3	2.9	5.3	0.1
Gypsum/Anhydrite	1.9	1.4	5.7	0.0
Fe-Oxides	1.6	1.7	0.4	0.0
Rutile	0.3	0.3	0.2	0.0
Other*	0.4	0.3	0.4	0.2
Total	100	100	100	100

*including amphibole, apatite, carbonates and ilmenite

Table 1B – Mineral distribution data used for gold deportment study from CIL leach stream

Mineral Mass	Sample ID		
(in wt%)	Feed	POX/CILResidue	CIL Residue
Quartz	51.1	52.0	49.7
Dolomite	26.0	27.2	27.5
Mica	6.3	5.7	6.6
Clay	9.0	8.6	10.1
Anhydrite/Gypsum	0.4	0.8	0.9
Pyrite	2.2	0.2	0.2
Calcite	3.0	3.7	4.1
Fe-Oxides	0.2	0.4	0.3
TCM	1.5	0.9	0.2
Others*	0.3	0.5	0.4
Total	100.0	100.0	100.0

The whole rock analysis, ICP scan for major elements, Au, S (t), S^{-2} and C-speciation analysis data indicate that the samples mostly composed silicates and carbonates. Gold assay was 3.27 g/t in feed, 3.22 g/t in Pox/CIL residue and 2.02 g/t in CIL residue. Organic carbon content ranges from 1.53% in feed to 0.23% in CIL residue. The assay results are presented in Tables 2–3.

Table 2A –Whole rock analysis data (wt.%) from flotation stream samples

Sample ID	SiO_2	Al_2O_3	Fe_2O_3	MgO	CaO	Na_2O	K_2O	TiO_2	P_2O_5	MnO	Cr_2O_3	V_2O_5
Rougher Feed	60.1	13.1	5.26	2.12	4.31	1.97	2.91	0.45	0.2	0.02	0.02	0.02
Rougher Tails	61.9	13.1	3.57	2.11	4.5	2.09	2.87	0.46	0.21	0.02	0.02	0.02
Cleaner Tails	42.5	13.8	16.3	2.18	3.57	1.38	3.24	0.48	0.22	0.02	0.09	0.02
Final Conc	1.47	0.55	43.28	0.17	< 0.05	0.04	0.12	0.1	<0.04	0.008	<0.004	<0.008

Table 2B – Whole rock analysis data (wt.%) from CIL Leach stream samples

Sample ID	SiO_2	Al_2O_3	Fe_2O_3	MgO	CaO	Na_2O	K_2O	TiO_2	P_2O_5	MnO	Cr_2O_3	V_2O_5	LOI
Feed	57.5	5.88	2.57	5.02	9.54	0.06	0.75	0.29	0.21	0.04	0.02	0.05	15
POX/CIL Residue	59.4	4.24	2.01	6.23	10.6	0.02	0.63	0.22	0.15	0.03	0.02	0.03	15.4
CIL Residue	55.8	6.12	2.56	5.56	11.3	0.07	0.7	0.26	0.18	0.04	0.01	0.04	16.1

Table 3A – Copper, gold and sulfur analysis data from flotation stream samples

Sample ID	Au (g/t)	Cu (%)	S^{-2} (%)
Rougher Feed	**0.23**	0.51	1.72
Rougher Tails	**0.04**	0.02	0.32
Cleaner Tails	**0.39**	0.19	10.3
Final Conc	**7.11**	33.2	30.8

Table 3B – Gold, sulfur and carbon analysis data from CIL leach stream samples

Sample ID	Au (g/t)	S^{-2} (%)	TCM (%)
Feed	8.34	1.08	1.53
POX/CIL Residue	3.36	0.07	0.89
CIL Residue	1.9	0.09	0.23

TCM Mineralogy

An optical microscopy study was carried out for morphological speciation and quantification of TCM. Based on this study and SEM-EDS compositional analysis, two broad categories of TCM were noted. The first category is the medium/coarse grained (20–50 µm) rectangular, triangular, sub-rounded TCM, occurred both as liberated and locked/attached to silicates or carbonates (Plate 2).

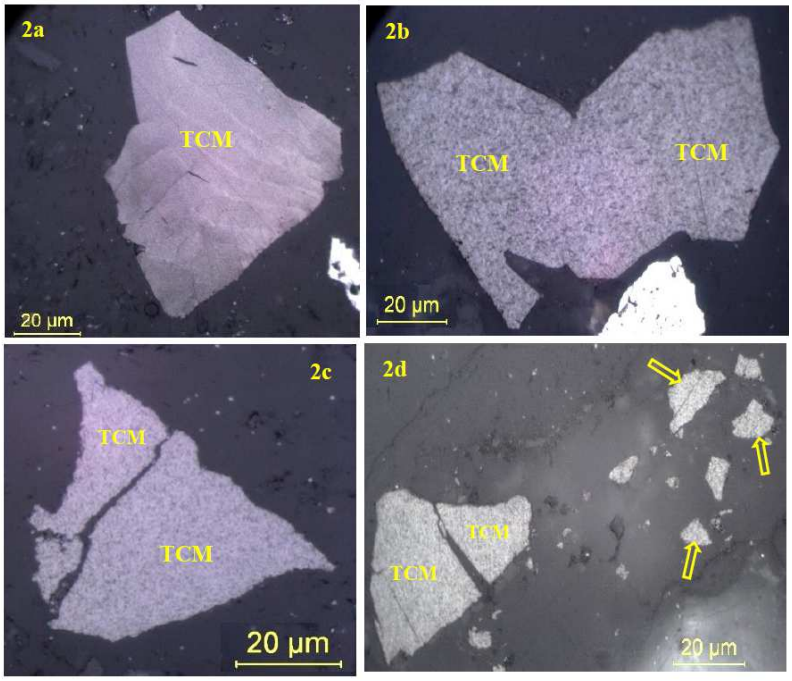

Plate 2 – Photomicrographs of polished sections from CIL leach stream samples under reflected light showing coarse to medium grained irregular carbonaceous matter (TCM and yellow arrow)

In general, this type of total carbonaceous material (TCM) is dominantly (>75%) composed of carbon with minor amounts of silicates, sulfides and iron oxides (Table 4).

Table 4 – SEM-EDS semi-quantitative analysis from coarse/medium grained TCM

Spots#	C	O	Al	Si	S	Fe
TCM1 #1	84.1	12.4	0.2	1	1.3	1
#2	86.2	11.1		0.5	1.1	1.1
TCM2 #3	77.5	15.3	0.4	2.4	1.2	3.2
#4	89.4	8		0.5	1	1.1

The second variety, of TCM is the fine grained disseminated (1–10 µm) elongated veins, veinlets or interstitial stringers, mostly locked within silicates/carbonates or occurs as composite TCM with silicates/carbonates, iron oxides and sulfides (Plate 2). The carbon content in this variety of TCM appears to vary widely from fractions of % to 50%, indicating the difficulty of analysis due to size constraints and mixed TCM/host mineral chemical spectra SEM-EDS analyses of both varieties of TCM and BSE images are given in Tables 4–5 and Plates 3–4.

Table 5 – SEM-EDS semi-quantitative analysis from fine grained composite TCM

Spots#	C	O	Na	Al	Si	S	Fe	Cu
TCM1 #1	27.1	24.7			39.1			9.1
#2	44.4	5.4		0.3	2.2	18.4	26.2	3.1
TCM2 #3	12.7	42.9	0.6	10.8	33			
#4	20.5	44		0.8	29.4	3	1	1.3

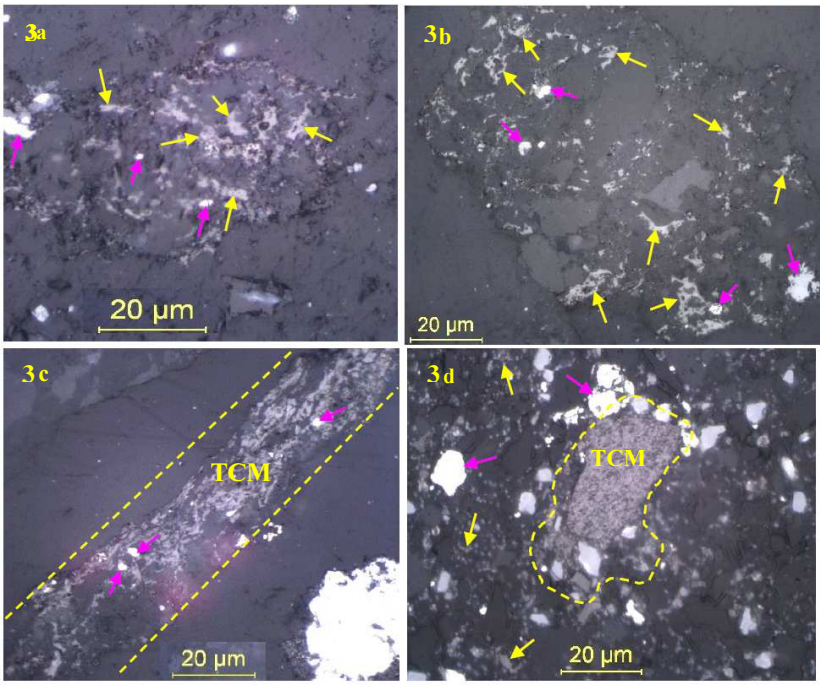

Plate 3 – Photomicrographs of polished sections under reflected light showing fine grained irregular bands, veins, and composite carbonaceous matter (TCM; yellow arrow) with silicates (Si) and pyrite (pink arrow)

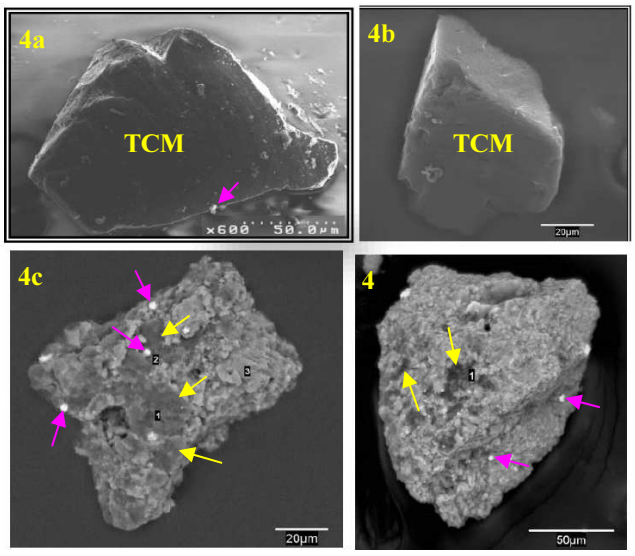

Plate 4 – BSE grain mount images of carbonaceous matter: a–b) coarse grained irregular rectangular TCM with pyrite inclusion (pink arrow); c–d) fine grained TCM (yellow arrow) within silicates (Si); also showing pyrite inclusions (pink arrow).

Electron Micro-Probe Analysis of TCM, Sulfides and Iron Oxides

Electron microprobe analysis for Au was carried out on TCM, sulfides (pyrite) and iron oxide phases with detection limit of 50–60 ppm for TCM, pyrite and for iron oxide/hydroxide phases. This technique was used for broad overview of gold concentration in TCM, pyrite and iron oxides using a Cameca Micro-probe system. The relatively high detection limit for Au provided by the electron micro-probe analysis was a major limitation to carry out an accurate quantitative analysis for invisible gold in mineral phases, in which the majority of invisible gold is present at concentrations below its detection limit. The study indicated the presence of some gold-bearing TCM, sulfides and Fe-oxides/hydroxides grains. The summary of the micro-probe analysis was presented in Table 6.

Table 6 – Summary of micro-probe trace-gold analysis data

Sample ID	Minerals	Total Number of Analysis	No. of analysis having Au-content ≥ D.L.	Au (g/t)	
				Max	Average
Feed	TCM*	52	23	381	78
	Pyrite	46	20	1005	123
	Goethite-Hematite**	40	15	203	64
POX/CIL Residue	TCM*	45	21	638	200
	Pyrite	40	16	1209	278
	Goethite-Hematite**	35	14	175	80
CIL Residue	TCM*	48	22	548	334
	Pyrite	35	14	754	149
	Goethite-Hematite**	32	12	160	70

* including composite TCM & pyrite inclusions within TCM

** including composite goethite/hematite & pyrite inclusions within goethite/hematite

Detailed analysis of carbonaceous particles for (Au, C, S, As, Fe, and Si) and back scattered imaging of micro-probe analysis spots were carried out (Plates 5a–d). This study indicated the presence of fine inclusions of sulfides, mainly, arsenian pyrite and pyrite within carbonaceous matter and also some composite carbonaceous matter, which accounted for most of the gold within carbonaceous particles. The gold content of some of composite TCM grains varied from ~200–600 ppm gold.

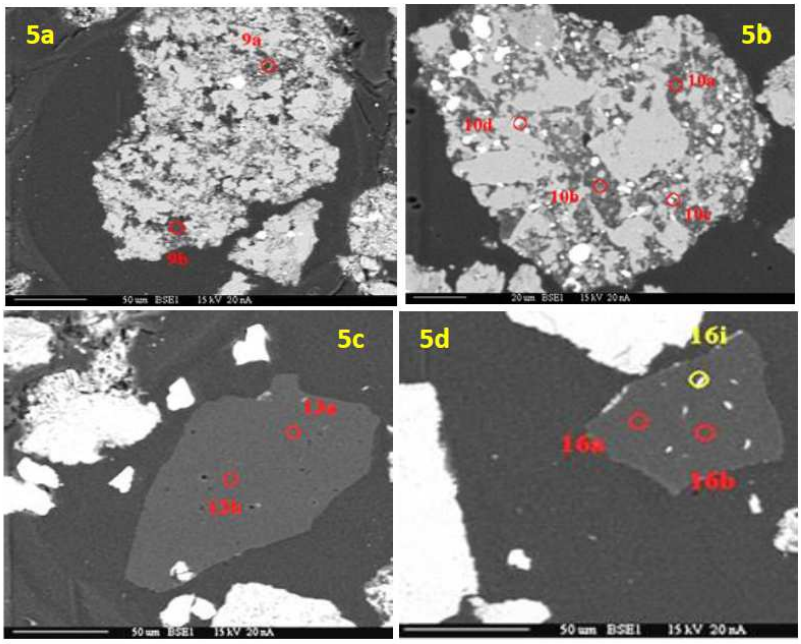

Plate 5 – BSE images of carbonaceous grains analyzed by micro-probe for trace gold, carbon and other elements: a–b) fine grained TCM and fine grained pyrite/iron-oxides inclusions within silicates; c) coarse grained TCM; and d) coarse grained TCM with pyrite inclusions

Gold Mineralogy

Visible Gold

Gold scans were carried out by optical microscopy and MLA for different polished sections prepared from all these samples after pre-concentration. A number of gold grains were noted from flotation stream samples while no visible gold grain was noted from CIL Leach stream samples (feed, POX and CIL residue). Gold grains were fine grained (average grain size 2–7 µm), mostly liberated in feed and concentrate samples and mostly locked in tailings (Table 7; Plates 6a–e).

Table 7 – Summary of visible gold grains from flotation stream samples

Sample ID	Number	Average Size (µm)	Composition Gold grains (Au%)	Measured Surface Area (in %)		
				Liberated	Attached	Locked
Feed	23	4	76 -95	61.2	26.2	12.6
Final Concentrate	430	7	77 - 98	89.9	8.9	1.2
Cleaner Scavenger Tail	4	3	80 - 92	0	0	100
Rougher Tail	5	2	84 - 85	0	23.1	76.9

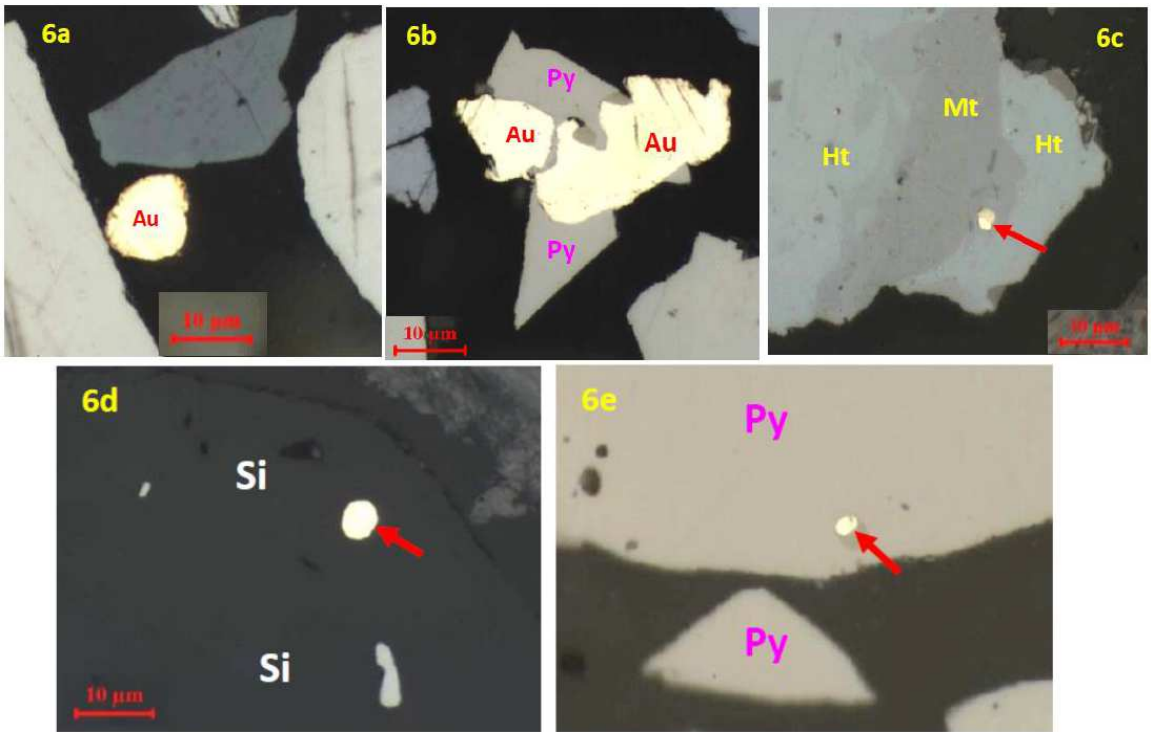

Plate 6 – Photomicrographs of gold grains: a) liberated gold grain (Au) in feed sample; b) attached gold grain (Au) in concentrate; c) locked gold grain (red arrow) in magnetite (Mt)-Hematite (Ht) from Ro tail; d) locked gold grain (red arrow) in silicates (Si) from Ro tail; and e) locked gold grain (red arrow) in pyrite (Py) from cleaner tail

Invisible Gold

Concentrations of invisible gold in sulfides, Fe-Oxides and TCM were determined using a Cameca IMS 3F SIMS instrument and the summarized data are presented in Tables 8A–B. Five different morphological types of pyrites were identified by optical microscopic study. Dynamic SIMS analysis was carried out for each of the varieties (Plate 7) to quantify global pyrite invisible gold concentration.

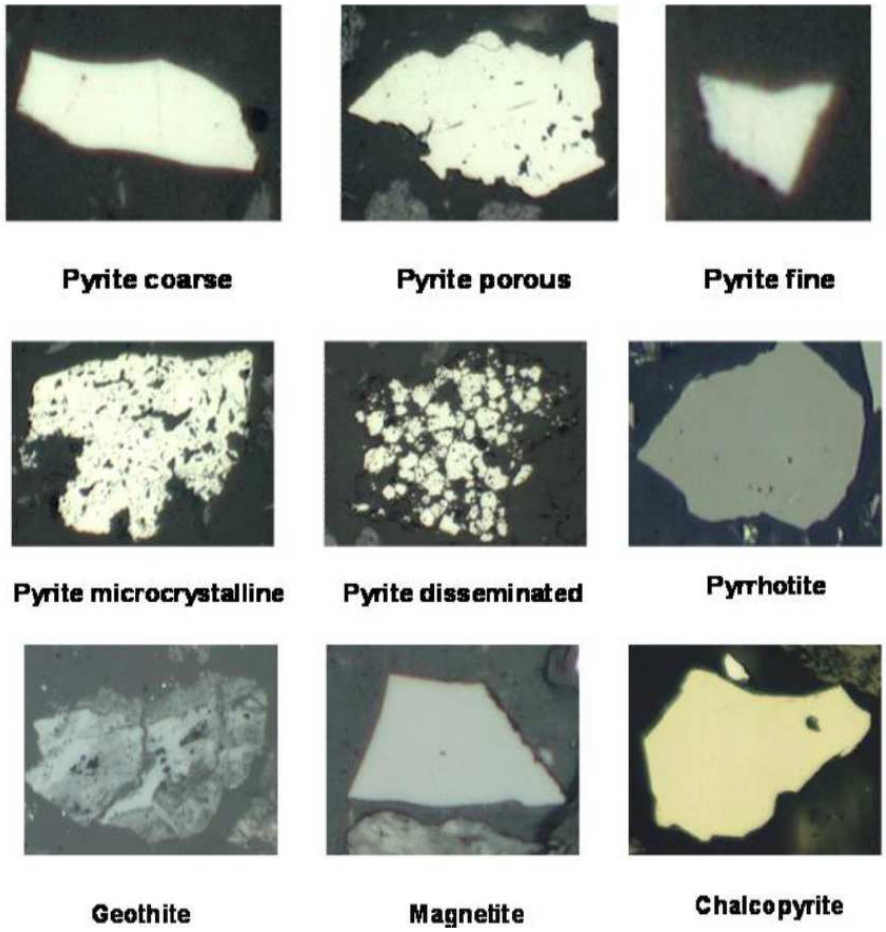

Plate 7 – Photomicrographs of different morphological types of pyrite grains, pyrrhotite, Fe-oxides and chalcopyrite analyzed by Dynamic SIMS

Invisible Gold in Sulfides and Iron Oxides

Dynamic SIMS analysis data from flotation stream samples indicate that pyrite was a minor gold carrier accounting for 2.5% in feed, 0.5% in concentrate, 0.34% in rougher tail and 8.6% in cleaner scavenger tail sample. Fe-oxides/hydroxides were a moderate gold carrier in two tails samples, with 12% in cleaner scavenger tail and 22.5% in rougher tail sample (Tables 8A–B).

SIMS data from CIL leach stream samples indicated that pyrite was the major gold carrier accounting for 86% in feed to 24% in POX/CIL residue samples (Table 9). Strong variability of the sub-microscopic gold concentration was observed between the different morphological types of pyrite. SIMS concentration depth profiles in microcrystalline/disseminated pyrite showed presence of 100% solid solution while 61% of the depth profiles in fine/porous pyrite showed solid solution gold and 39% as colloidal type gold. All measured coarse pyrite grains carried only colloidal type gold.

Table 8A – Measured invisible gold concentrations in sulfides and Fe-oxides from flotation stream samples

Sample ID	Minerals	Pyrite			Chalcopyrite	Other Cu-sulphides	Galena	Fe-Oxides
	Morphology	Coarse	Fine	Porous	Coarse/Medium	Medium	Medium	Coarse/Medium
Feed	Range (ppm)	0.75-3.71	0.47-5.72	0.97-21.16	0.96-3.95	0.85-5.18	0.36-1.74	0.60-3.05
	Average (ppm)	1.44	1.73	3.49	1.9	2.52	0.81	1.35
Final Conc	Range (ppm)	0.42-3.58	0.5-4.97	0.87-8.28	0.69-4.00	0.35-15.94	0.18-2.92	0.58-1.69
	Average (ppm)	1.37	1.99	2.93	1.78	4.41	1.19	1.13
Cleaner Scavenger Tail	Range (ppm)	0.70-2.53	0.56-3.20	0.87-4.67	0.63-5.96	-	0.29-3.40	0.52-3.09
	Average (ppm)	1.17	1.34	2.1	1.69	-	0.82	1.3
Rougher Tail	Range (ppm)	0.72-1.57	-	0.83-14.98	0.53-2.95	1.31-3.97	-	0.44-2.89
	Average (ppm)	1.14	-	5.38	1.56	2.85	-	1.17

Table 8B – Visible gold and invisible gold distribution in sulfides and Fe-oxides phases from flotation stream samples

Sample ID	In-visible/Sub-microscopic Gold (in %)				Visible/Microscopic Gold (in %)
	in Pyrite	in Cu-sulphides	in other Sulphides	in Fe-Oxides	
Feed	2.46	2.64	0.04	5.54	89.32
	Total in-visible gold: 11%				
Final Concentration	0.47	4.53	0.09	0.02	94.89
	Total in-visible gold: 5%				
Cleaner Scavenger Tail	8.59	0.3	0.09	11.93	79.09
	Total in-visible gold: 21%				
Rougher Tail	0.34	1.04	-	21.49	77.13
	Total in-visible gold: 23%				

Table 9 – Measured invisible gold concentrations in sulfides and Fe-oxides from CIL leach stream samples

Sample ID	Minerals	Pyrite			Microcrystalline/disseminated	Fe-Oxides
	Morphology	Coarse	Fine	Porous	Pyrite aggregates	
Feed	Average (ppm)	4.31	127.68	155.6	470.19	3.75
	Range (ppm)	0.4 – 6.0	13 - 430	6 - 470	52 - 1330	0.14 - 10
	Distribution (%)	**0.21**	**17.2**	**12.65**	**55.74**	**0.14**
POX/CIL Residue	Average (ppm)	3.9	121.86	141.72	444.77	3.91
	Range (ppm)	0.7 – 7.9	15 - 247	75 - 251	96.9 – 938.3	0.48 – 9.8
	Distribution (%)	**0.01**	**4.81**	**5.53**	**12.59**	**0.41**
CIL Residue	Average (ppm)	3.2	115.85	158.8	466.23	3.75
	Range (ppm)	0.8 – 5.7	21.6 - 245	32.7 -367	54.5 - 1175	0.48 – 13.8
	Distribution (%)	**0.02**	**3.66**	**4.85**	**10.72**	**0.59**

Preg-Robbed Surface Gold in Carbonaceous Matter

The TOF-SIMS analytical technique was used to detect and speciate different forms of surface gold on carbonaceous matter and to characterize the preg-robbing properties of different forms of carbonaceous matter. Two different sets of samples were prepared for this analysis: (i) as received feed sample and (ii) feed sample doped with controlled amount of $Au(CN)_2$. TOF-SIMS analysis on the first set of particles was used to determine the presence of different forms of surface gold on "as received" TCM grains. TOF-SIMS analysis on the second set of doped feed samples was used to characterize the preg-robbing properties of different types of TCM. Due to the low molecular fragmentation during the TOF-SIMS analysis, this techniques measured simultaneously the presence of Au in both elemental (Au^0) and compound forms such as $Au(CN)_2$, $AuCl_2$ or $Au(S_2O_3)_2$. The quantification of the TOF-SIMS data was based on element and compound specific standards with established detection limits for surface metallic and compound gold in the low ppm range (Dimov, Hart, & Chattopadhyay, 2009).

All identified types of carbonaceous matter showed preg-robbing capacity. The TOF-SIMS analysis showed substantial pre-robbing capacity of the carbonaceous material present in feed sample and high variability in preg-robbed surface gold largely due to the amount of disseminated carbon present or exposed on the surface of various grains.

Raman spectroscopic analysis of carbonaceous grains indicated that the structure of both coarse grained and fine disseminated carbonaceous matter was similar to that of natural activated carbon. The results from the Raman analysis for both types of carbonaceous grains are presented in Plate 8.

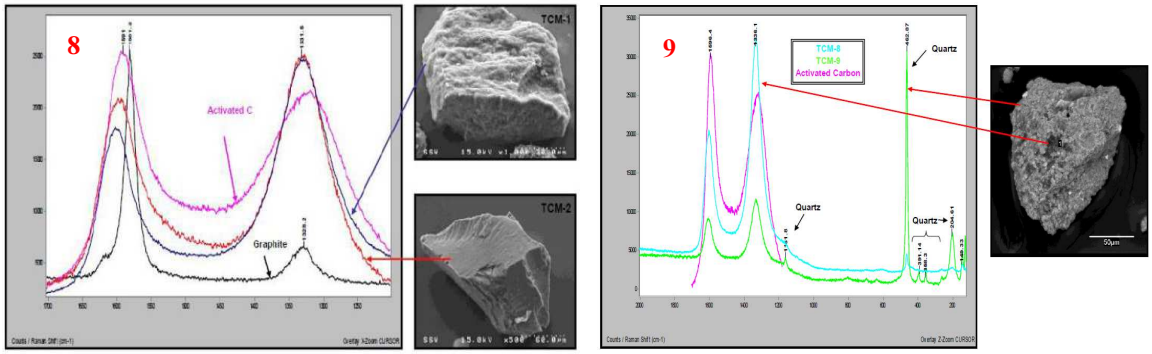

Plate 8 – BSE image and Raman spectra of activated carbon, graphite, and coarse and fine grained TCM

The TOF-SIMS analysis of as received carbonaceous matter from the feed sample did not show a presence of metallic surface gold above the minimum detection limit of 2–5 ppm while elevated concentrations of surface gold on carbonaceous matter from POX-CIL and CIL residue samples were observed by TOF-SIMS. The results of preg-robbed surface gold from POX-CIL and CIL residue samples are presented in Tables 10–11.

Table 10 – Preg-robbed Surface Gold in POX/CIL Residue by TOF SIMS Analysis

Sample ID	Carbonaceous matters	Estimated Preg-robbed surface Au (in ppm)	Surface Gold Distribution (%)	Total Preg-robbed Surface Au (%)
	Fine grained disseminated	0.27	12.4	
POX/CIL Residue	veins/stringers			**64.8**
	Coarse grained	1.43	52.4	
	rectangular/triangular			

Table 11 – Preg-robbed Surface Gold in CIL Residue by TOF SIMS Analysis

Sample ID	Carbonaceous matters	Estimated Preg-robbed surface Au (in ppm)	Surface Gold Distribution (%)	Total Preg-robbed Surface Au (%)
	Fine grained disseminated	0.2	10.7	
CIL Residue	veins/stringers			**54.2**
	Coarse grained	0.94	43.5	
	rectangular/triangular			

RESULTS AND DISCUSSION

Gold deportment is the key aspect of this work. Complete details will not be presented here due to the proprietary nature of this work. An accurate mass balance of gold in various mineral species, including visible and invisible gold, is not trivial and requires significant experience and expertise. The need for understanding the errors associated with various measurement steps is crucial as there is potential for significant errors in gold deportment if not carried out meticulously.

For quantification of invisible gold in different sulfides and Fe-Oxides, dynamic SIMS data for average concentration of gold in these phases, mineral abundances from XRD, optical microscopy and QEMSCAN were applied (Chattopadhyay & Gorain, 2013). The quantitative gold deportment study on flotation stream samples indicated total sub-microscopic gold was 11, 5, 21, and 23% for feed, concentrate, scavenger tail and rougher tail, respectively. In feed sample, sulfides and iron oxide phases accounted for 5.5% each of total gold, while copper sulfides accounted for most of the sub-microscopic gold (4.5%) in the concentrate. In scavenger tail, sulfides and Fe-oxides accounted for 9 and 12% of total gold, respectively, and in rougher tail sample Fe-Oxides accounted for 22% of the total gold.

In CIL leach stream samples both Dynamic SIMS and TOF-SIMS data were utilized for the quantification of surface preg-robbed gold in carbonaceous matter. Aggregates of disseminated/ microcrystalline pyrite were a major carrier of gold accounting for 56% of the total gold in feed sample (Table 10). Porous and fine pyrite grains were minor gold carriers accounting for 17 and 13% of total gold, respectively. No preg-robbed surface gold was noted in feed sample.

Preg-robbed surface gold in carbonaceous matter (TCM) was the major gold carrier accounting for 55–65% of total gold in POX/CIL residue samples (Table 10). Most of the preg-robbed surface gold (52%) was noted on coarse grained rectangular/triangular TCM, while fine grained disseminated veins/stringers of TCM accounted for about 12% of the gold. Aggregates of disseminated and microcrystalline pyrite were the minor carriers of gold accounting for 13% of the total gold in the cleaner scavenger tail (Table 8). Porous and fine pyrite grains were minor carriers accounting for 5% each.

In CIL Residue sample, preg-robbed surface gold in TCM was the major gold carrier accounting for 54% of total gold (Table 11). Most of the preg-robbed surface gold (43%) was noted on coarse grained TCM, while fine grained disseminated stringers of TCM accounted for about 11% gold. Aggregates of disseminated/microcrystalline pyrite were minor carriers of gold accounting for 11% of total gold (Table 8). Porous and fine pyrite grains were minor carriers accounting for 5 and 4%, respectively.

This gold deportment study provides the key input required for mass balancing the flow of gold associated species (invisible and preg-robbed surface gold) across the leach circuit. Though difficult in some cases, this is an important step after the mineralogy work is typically completed. It is of key importance to obtain a detailed view of recovery of gold across the leach circuit, which is critical for metallurgy diagnostics.

CONCLUSIONS

This paper discusses the various steps and processes involved in carrying out a quantitative gold deportment study for complex copper-gold and double refractory gold ores. Though challenging, this study provides useful information for optimization of metallurgical processes. The gold deportment study presented in this paper highlighted the key source of gold losses in flotation tailings and POX/leach residues. Fe-oxides (goethite, hematite and magnetite) accounted for 12 and 22% of total gold in cleaner scavenger and rougher tails, respectively, which is not common in flotation stream samples. Carbonaceous matter, fine inclusions of pyrite and arsenean pyrite and preg-robbed surface gold accounted for unusually high gold losses, which is not typical for many gold leaching operations. Pre-robbed surface gold accounted for 65% and 54% of the total gold in the POX residue and CIL residue samples.

The findings of this gold deportment study were immensely useful for Barrick in clearly identifying and quantifying the gold losses in the two tailings streams. Metallurgical recovery strategies were initiated to maximize gold recovery which is beyond the scope of this work.

ACKNOWLEDGMENTS

The authors are grateful to Barrick Gold Corporation for sponsoring this work and for their permission to publish this paper. Sincere thanks to Process Research Ortech Inc. and SGS Minerals Inc. for their support in some mineralogy work, along with Dr. Marc Choquette of Laval University, Lori Kormos of Xstrata and Wendy Ma of Inspectorate, for providing their expertise from time to time.

REFERENCES

Arehart, G.B. Chakurian, A.M., Tretbar, D.R., Christensen J.N., McInnes, B.A., & Donelick, R.A. (2003). Evaluation of radioisotope dating of carlin-type deposits in the Great Basin, western North America, and implications for deposit genesis. *Economic Geology*, 98(2), 235–248.

Bettles, K. (2002). Exploration and geology, 1962 to 2002, at the Goldstrike Property, Carlin Trend, Nevada. Society of Economic Geologists Special Publication No. 9, 275–298.

Chattopadhyay, A., and Gorain, B. (2013). Gold deportment studies on a copper gold ore – A systematic approach to quantitative mineralogy focusing on diagnostic metallurgy. *45th Annual Canadian Mineral Processors Operators Conference*, Ottawa, ON, 29–42.

Chattopadhyay, A., & Gorain, B. (2014). A novel approach to quantify gold deportment for double refractory gold ores. *XXVII International Mineral Processing Congress (IMPC-2014)*, Santiago, Chile.

Dimov, S.S., Hart, B.R., & Chattopadhyay, A. (2009). Speciation and quantification of surface gold in carbonaceous matter from AC POX stream products by TOF-SIMS Mineralogy. *Proceedings of the 48th Annual Conference of Metallurgists of CIM*, Sudbury, ON, 85–91.

Hausen, D.M., & Bucknam, C.H. (1984). Study of preg-robbing in the cyanidation of carbonaceous gold ore from Carlin, Nevada. *Proceedings of International Congress on Applied Mineralogy in Mineral Industry*, Los Angeles. Park, W.C., Hausen, D.M., Hagni, R.D., (eds.). Metallurgical Society of American Institute of Mining, Metallurgical, and Petroleum Engineers, 833–856.

Helm, M., Vaughan, J., Staunton, W.P., & Avraamides, J. (2009). An investigation of the carbonaceous component of preg-robbing gold ore. *World Gold Conference 2009*. The Southern African Institute of Mining and Metallurgy, 139–144

Jensen, E.P., & Barton, M.D. (2000). Gold deposits related to alkaline magmatism. *Reviews in Economic Geology, 13*, 270–314.

Sillitoe, R.H., & Perelló, J. (2005). Andean copper province - Tectonomagmatic settings, deposit types, metallogeny, exploration and discovery. *Economic Geology 100th Anniversary Vol.,* 845–890.

Stenebraten, J.F., Johnson, W.P., & McMullen, J. (2000). Characterisation of Goldstrike ore carbonaceous material, part 2: Physical characteristics. *Mineral and Metallurgical Processing, 17*(1), 7–15.